Applied Geochemistry 168 (2024) 106029

Contents lists available at ScienceDirect

Applied Geochemistry

journal homepage: www.elsevier.com/locate/apgeochem

Environmental impacts and risk assessment in the re-use of Cr-bearing pyrolyzed tannery wastes: A case study in a residential area

Lisa Ghezzi [a,*], Simone Arrighi [a], Enrico Mugnaioli [a], Natale Perchiazzi [a], Erika Zamponi [a], Simone Pollastri [b], Fabrizio Franceschini [c], Riccardo Petrini [a]

[a] Department of Earth Sciences, University of Pisa, Via S. Maria 53, 56126, Pisa, Italy
[b] Elettra - Sincrotrone Trieste, in AREA Science Park, 34149, Basovizza, Trieste, Italy
[c] Environmental Protection Agency of Tuscany (ARPAT), Via Vittorio Veneto, 56127, Pisa, Italy

ARTICLE INFO

Editorial Handling by: Dr V Ettler

Keywords:
Tannery waste recycling
Hexavalent chromium
Risk analysis
Leather sludge pyrolysis
KEU

ABSTRACT

Increasing concern has been raised on the environmental impacts of chromium-tanning wastes recycling. In particular, the pyrolytic conversion of leather industry sludges into Cr(VI)-free carbonized residues is believed to represent a viable route for a sustainable re-use of this type of wastes. The aim of this study was to determine the impact of recycled Cr-bearing pyrolyzed char (named KEU) as backfilling material for road construction in an urban area in Tuscany (Italy). Geochemical and chromium-isotope data, together with microstructural analyses (HR-TEM and XAS), indicate that the presence of KEU results in a significant enhancement of the natural Cr background. The results support the hypothesis that, in environmental conditions, the Cr (III) hosted in KEU is converted into Cr(VI), which is leached out by rainwater. Indeed, Cr(VI) is dispersed in surface water, reaching concentrations up to 18 mg/L and it also occurs in coatings on the surface gravel of unpaved roads. The $^{53}Cr/^{52}Cr$ ratio measured in KEU, reported in $\delta^{53}Cr$ notation, was in the restricted range $\delta^{53}Cr = -0.031 \pm 0.057$ ‰; on the contrary, the $\delta^{53}Cr$ in water varied between $+1.581 \pm 0.038$ ‰ and $+3.261 \pm 0.191$ ‰, indicating the reduction of Cr(VI) after the pristine oxidative mobilization. The risk-based soil screening levels (SSLs) for total Cr are well above the concentration measured in soil for all the exposure pathways. On the contrary, the SSL for Cr(VI)indicates that soil contamination poses health hazards for residents.

1. Introduction

The management and reuse of wastes as secondary raw materials for a sustainable circular economy aims at retaining resources within value chains, reducing negative environmental impacts (Das et al., 2019; Bongers and Casas, 2022). Despite the development of cleaner technologies (Rosu et al., 2018; China et al., 2020), leather tanning still represents a potentially pollution-intensive industry (Dixit et al., 2015; Laurenti et al., 2016), generating substantial quantities of hazardous non-renewable waste by-products (Sivaram and Barik, 2019; Tasca and Puccini, 2019). In particular, the chromium salts (usually basic Cr(III) sulfate), used as tanning agent in over 80% of the world's leather production, produce a tannery sludge with Cr excess, yielding potential negative environmental impacts when wastes are improperly treated and disposed (Mella et al., 2015; Famielec, 2020). Tannery sludge thermal decomposition represents a way to recover leather waste as secondary raw material; in particular, pyrolysis treatments (Arcibar-Orozoco et al., 2022) fix the potentially toxic Cr(III) into solid phases that are considered stable in the environment (Guan et al., 2019). It is hence generally assumed that the carbonized products of wastes obtained by pyrolysis, free from toxic Cr(VI), are less hazardous than the original waste and can be used for a variety of applications, in a closed-loop economy model (Chojnacka et al., 2021; Verma and Sharma, 2022). However, when this material is reused in environmental settings, it is necessary to ensure that Cr(III) in the pyrolyzed wastes remains resistant to oxidation to the highly toxic hexavalent form over long periods of time (Apte et al., 2005).

Italy is an important player in the leather market. In particular, the tanning district of Santa Croce sull'Arno (Tuscany Region), comprising more than 250 small and medium sized companies, is one of the largest tanning districts in Europe. A pyrolysis plant was built to solve the environmental issues related to landfill disposal of the whole tanning sludge produced by the district, improving the environmental sustainability of the tanning process. The plant can treat up to about 500.000

* Corresponding author.
E-mail address: lisa.ghezzi@unipi.it (L. Ghezzi).

https://doi.org/10.1016/j.apgeochem.2024.106029
Received 18 December 2023; Received in revised form 26 March 2024; Accepted 26 April 2024
Available online 28 April 2024

Fig. 1. Location and urban setting of the Green Park construction site, a housing project approved by the local government (www.pontederaparcoverde.com).

m^3/y of sludge flow. In the plant, the tannery sludge is first dehydrated by centrifugation and the residue is dried by air blowers at 250 °C to obtain about 90 % of total solid content. The solid that forms is then pyrolyzed at 900 °C and sintered at 1000–1100 °C by methane/oxygen burners, adopting a stoichiometric oxygen/methane ratio to prevent Cr oxidation, given that, during pyrosintering, chromium is totally converted into its trivalent form. The resulting high-temperature material is finally cooled by spraying water to produce a carbonaceous granulate (called KEU) with particle size ranging from about 0.5 mm to 4 mm. Leaching tests highlighted that, at the time of production, KEU does not contain detectable amounts of Cr(VI) (<0.5 mg/kg) (Ghezzi et al., 2023). KEU obtained the European Waste Code legal classification 19 01 12 (mirror non-hazardous), essentially based on leachate analysis. As a reusable resource, KEU was mixed with demolition wastes (code EN 13242:2002 + A1:2007 Unbound aggregates for use in civil engineering and road construction) and recycled as inert filler for road construction and in excavated areas. This material will be called KEU-bearing aggregate.

Groundwater monitoring in the sites of KEU-bearing aggregate disposal revealed severe hexavalent chromium contamination, suggesting that the recycled KEU was becoming an environmental source for Cr(VI). Indeed, recent microstructural studies (Ghezzi et al., 2023) revealed that trivalent chromium in KEU partially formed oxides and/or hydroxides that were prone to oxidize over time in air and wet conditions, making the KEU-bearing aggregate a potential source of hexavalent chromium when exposed to ordinary ambient conditions and upon aging.

In the present study, the environmental impact of the reuse of KEU-bearing aggregate in a site intended for residential use in a densely populated urban area in Tuscany is evaluated. In particular, the fate of Cr(VI) contamination and the risk posed to human health are addressed.

2. Study site

The study site is located within the Pontedera Municipality, in the Tuscany Region (Italy). A new urban residential neighborhood, called

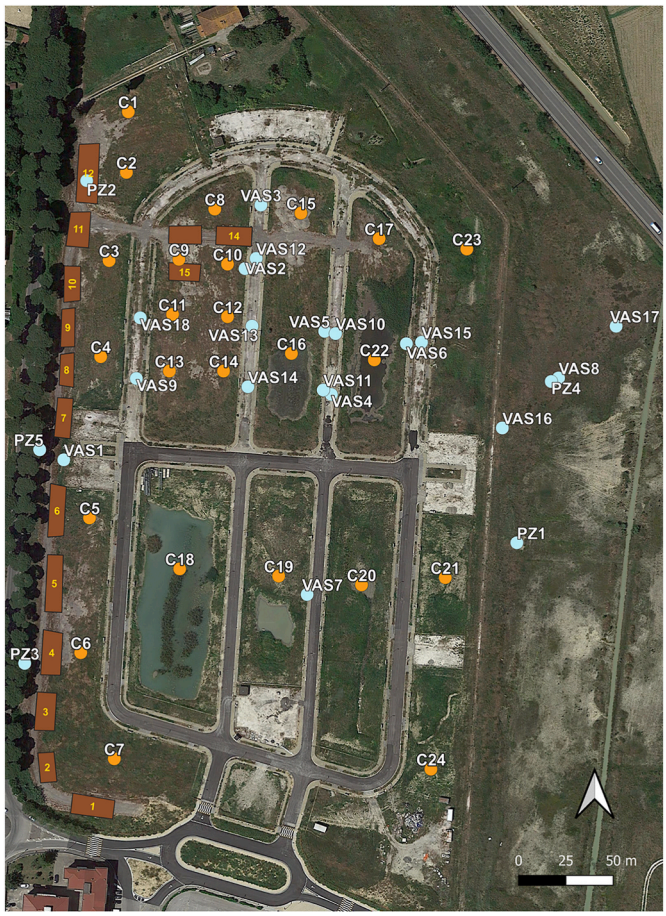

Fig. 2. Sampling stations at the Green Park area. Labels are: PZ: piezometers; VAS: storage tanks at nodes in the runoff drainage system; C: soil samples; 1–15 numbered boxes: stockpiles of Cr-bearing aggregate.

Green Park, was planned in this site which is contiguous with the existing urban area (Fig. 1).

Construction work at Green Park began in 2013. The landscape characteristics of the site were heavily modified by excavation, landfilling, levelling and grading, in order to comply with building regulations. While preparing the site for construction, a fence was installed to secure the area, and a road for the access of heavy equipment machinery was built; the road was made using approximately 5500 tons of KEU-bearing aggregate. In April 2018 a land survey performed by the Agency for Environmental Protection of Tuscany Region revealed soil contamination by total chromium (ARPAT; register # 0029118, April 23, 2018). Later, Cr(VI) was detected in the shallower groundwater, where it largely exceeded the 5 μg/L threshold imposed by Italian regulations (Legislative Decree 152/2006). A stop work order was issued suspending the construction work until the source and fate of contamination were adequately identified and the problem solved. At present, activities at the site are still not authorized. This was detrimental to project margin and timeline, leading to costly and time-consuming problems for builders and contractors.

In order to reduce the possible Cr(VI) leaching from the KEU-bearing aggregate by rainwater and for site clearance purposes, on September 2022 the road made of KEU-bearing aggregate was removed by backhoe loaders to form 15 waste piles, later capped by plastic material keeping them in place.

The natural soil in the site is composed of alternating sub-horizontal centimeter to decimeter thick deposits of loamy sands and silty layers. Lateral heteropies characterize the profile. In this area, a deep groundwater aquifer confined in sandy alluvial layers and used as drinking

Table 1
Recommended exposure factors (ISPRA, 2008; US EPA, 2014; US TCEQ, 2023).

Symbol	Definition	Value
IR_{ing}	Ingestion rate (mg/day) (accounting for both soil and dust ingestion)	100 for adult ($IR_{ing\text{-}a}$), 200 for children ($IR_{ing\text{-}c}$)
EF	Exposure frequency (day/year) for residential setting	350
ED	Exposure duration (years) for residential setting	24 for adults (ED_a), 6 for children (ED_c)
SA	Exposed skin area (cm^2)	5700 for adults (SA_a), 2800 for children (SA_c)
SAF	Skin adherence factor (mg/cm^2)	0.07 for adults (SAF_a), 0.2 for children (SAF_c)
ABS	Dermal absorption factor (fraction of contaminant absorbed dermally from soil, unitless)	0.01 (chemical specific)
BW	Average body weight (kg)	70 for adults (BW_a), 15 for children (BW_c)
AT (Ingestion and dermal contact)	Average time of exposure (day)	ED × 365 day/year for non-carcinogens, 70 year (lifetime) × 365 day/year for carcinogens
AT (inhalation)	Average time of exposure (h)	ED × 365 day/yr × 24 h/day for non-carcinogens, 70 years × 365 days/year × 24 h/day for carcinogens
RBA	Relative bioavailability factor (unitless)	chemical specific, in the absence of data was assumed to be equal to 1
ADAF	Age-dependent adjustment factor	5 for 0–6 years of age, 1 for 6–30 of age

Table 2
Concentration of trace elements considered (mg/kg) in KEU-bearing aggregate together with the maximum concentration level (MCL, mg/kg) imposed by Italian regulations for residential soil. Values in bold exceed the MCL.

Sample	P1	P2	P3	P4	P5	P6	MCL
Sb	**27**	**19**	**34**	**28**	**39**	**27**	10
As	9.8	9.7	13	11	12	10	20
Be	0.9	1	1	0.8	0.9	0.8	2
Cd	1.5	1.6	**2.8**	1.6	**2.5**	1.6	2
Co	**103**	**21**	**21**	14	16	17	20
Cr_{tot}	**6267**	**3388**	**8384**	**7356**	**7808**	**5289**	150
Cr(VI)	**22**	**7.8**	**15**	**17**	**10**	**4.7**	2
Fe	59901	49770	73989	69541	73563	54937	
Mn	611	846	832	666	676	682	
Hg	0.2	0.5	0.3	0.7	0.6	0.5	1
Ni	66	59	83	67	94	65	120
Pb	83	99	**108**	**105**	**119**	98	100
Cu	**282**	**272**	**335**	**328**	**364**	**266**	120
Se	**3.3**	2.8	**5.7**	2.5	**5.2**	**3.1**	3
Tl	0.1	0.2	0.1	0.1	0.2	0.1	1
V	36	38	42	38	41	34	90
Zn	**742**	**566**	**1170**	**1407**	**703**	**576**	150
<2 mm fraction (%)	61.2	65.5	66.9	61.4	65.4	61.1	

water supply is overlaid by shallower unconfined water-table aquifers.

3. Materials and methods

Sampling stations for KEU-bearing aggregate, soil, surface water and groundwater are shown in Fig. 2.

3.1. Sampling and analysis of solid materials

Samples from the 15 KEU-bearing aggregate stockpiles (Fig. 2), collected during a survey in 2022, were mixed together to form P1 to P7 composite samples (P1: stockpiles 1–2; P2: stockpiles 3–4; P3: stockpiles

Table 3
Concentration of trace elements considered (mg/kg) in soil. Values in bold exceed the maximum concentration level (MCL, mg/kg, see Table 2) imposed by Italian regulations for residential soil.

	C1	C2	C3	C4	C5	C6	C7	C8	C9	C10	C11	C12	C13	C14	C15	C16	C17	C18	C19	C20	C21	C22	C23	C24
Cr_{tot}	**512**	73	138	**228**	**661**	**320**	72	**642**	**699**	**238**	**1290**	**343**	**2130**	**2250**	**4170**	**1030**	133	82	**210**	114	150	84	86	**174**
Ni	51	**1030**	39	47	54	42	52	56	38	38	62	54	54	59	63	58	53	72	34	46	46	61	75	86
Cu	59	**199**	32	51	74	41	31	**138**	115	47	88	92	100	**135**	**783**	**850**	31	34	26	33	43	51	35	49
Zn	145	76	72	**166**	**242**	131	82	**523**	**176**	128	**222**	**342**	**256**	**259**	**2390**	**165**	78	87	66	83	96	82	95	117
As	9	6.7	5.9	8.3	8.1	7.3	7.2	6	5.6	7.3	9	10	7.6	7.9	7.4	5.8	7.8	7.5	6.1	7.2	7.6	8.1	**19**	9
Cd	<1	0.1	0.2	0.4	1.5	0.5	0.5	1.1	0.7	0.8	1.3	**4.5**	1.9	1.3	0.8	0.8	0.3	0.3	0.4	0.2	0.3	0.3	0.4	0.4
Pb	40	14	34	47	43	46	23	48	53	55	46	42	41	38	115	38	28	15	15	**104**	35	23	17	22
Co	11	**1540**	9.1	17	10	9.4	11	8.3	7.3	8.4	11	13	9.6	9.8	9.4	9.1	7.5	16	7.5	11	10	14	16	18
V	56	48	34	36	33	34	41	23	28	33	34	31	27	28	24	30	24	62	28	42	41	51	64	71
Be	1.2	1	0.7	0.8	0.8	0.7	0.9	0.5	0.7	0.7	1.0	1.0	0.8	0.7	0.4	0.7	0.5	1.4	0.6	0.8	0.8	1.1	1.4	1.6
Hg	<0.1	<0.1	0.1	0.2	0.3	0.2	<0.1	0.2	0.2	0.2	0.4	0.1	0.3	0.3	0.6	0.2	0.1	0.1	<0.1	0.1	0.1	0.1	0.1	0.1
Sb	**12.0**	3.0	3.0	4.0	7.0	3.0	<2	**16.0**	**12.0**	**22.0**	**15.0**	8.0	**25.0**	**17.0**	**49**	2.0	**13.0**	**17**	<2	2	<2	<2	3	<2
Se	<1	<1	<1	<1	<1	<1	<1	<1	<1	<1	<1	3	6	1	<1	<1	<1	<1	<1	<1	<1	<1	<1	<1
Cr(VI)[a]	7.3	6.6	2.6	4.8	16.4	15.7	5.5	1.5	31	22	14.8	25	30	29	9.6	nd	19.3	nd	1.4	11.4	1.9	nd	0.9	1.9
<2 mm fraction	nd	98.7	76.9	74.9	76.2	74.9	87.6	71.3	67.3	75.6	76.9	76.3	79.9	80.6	66.4	70.7	83.5	99.4	77.3	78.9	79	91.6	98.7	97.8

nd = not determined.
[a]Measured on top-soil (0–5 cm) collected during 2024 to evaluate the present-day hexavalent Cr contamination.

Table 4
KEU-bearing aggregate leaching tests.

Sample		P1-L	P2-L	P3-L	P4-L	P5-L	P6-L	P7-L
EC	µS/cm	1875	1051	1460	1916	1619	1937	1714
F	µg/l	<0.50	<0.25	<0.50	<0.50	<0.50	<0.50	<0.50
Cl	mg/l	32.8	45.2	26.4	18	54.1	38.8	23.9
SO_4	mg/l	1184	535	866	1229	877	1195	990
Sb	µg/l	21	16	19	18	21	18	17
As	µg/l	1.2	1.8	<1	<1	1.1	<1	1
Ba	µg/l	28	26	28	27	31	29	30
Cd	µg/l	<0.05	<0.05	0.05	<0.05	<0.05	<0.05	<0.05
Cr_{tot}	µg/l	1880	715	1410	1860	944	390	530
Cr(VI)	µg/l	1830	700	1395	1780	940	375	520
Hg	µg/l	<0.1	<0.1	<0.1	<0.1	<0.1	<0.1	<0.1
Mo	µg/l	30	22	26	29	29	28	26
Ni	µg/l	<1	<1	<1	1.2	<1	1.1	<1
Pb	µg/l	<1	<1	<1	<1	<1	<1	<1
Cu	µg/l	1.4	1.9	2.1	2.1	2	1.7	1.9
Se	µg/l	1.6	1.8	2.1	1.6	1.9	2.1	1.7
Tl	µg/l	<0.05	<0.05	<0.05	<0.05	0.05	<0.05	<0.05
Zn	µg/l	1.3	<1	2.1	2.6	2	1.7	1.9

5–6; P4: stockpiles 7–8; P5: stockpiles 9–10; P6: stockpiles 11–12; P7: stockpiles 13-14-15). Soil was sampled in a 2018 survey in 24 stations (samples C1 to C24, Fig. 2) throughout trenches about 1 m deep, made using a ditching machine, obtaining 1 kg composite samples. The 0–5 cm top-soil in 21 of the original 24 stations was collected during 2024, in order to evaluate the present-day hexavalent chromium contamination level.

Samples were quartered and dry sieved to separate the <2 mm fraction for multi-element chemical analysis, as required by Italian regulations. The separation of soil skeleton (>2 mm fraction) from the fine earth was achieved by dry sieving (Corti et al., 1998).

Gravels of different sizes used as stone base in roadways under construction, planned to provide secondary connections and access to the different properties in the Green Park residential area, were also taken. These materials are characterized by widespread greenish coatings, that were gently scraped and collected.

The concentration of trace elements in the stockpiled KEU-bearing aggregate and soil was determined by applying the EPA 3051 A (2007) + EPA 6010D (2018) methods, except mercury that was analyzed by the EPA 7473 method (2007). Hexavalent chromium in 2024 soil samples was selectively extracted by using 0.1 M Na_2CO_3 (Panichev et al., 2003; Elci et al., 2010).

To assess the release of pollutants to water, leaching tests were performed following the compliance test for leaching EN 12457–2:2002. The extractable Cr(VI) from gravel coatings during runoff was determined using monolithic leaching batch tests, where only the sample's outer surface was exposed to water. Tests were performed for 48 h and 7 days using Milli-Q water.

Coatings were analyzed by X-ray powder diffraction using a Bruker D2 phaser diffractometer, equipped with a Lynxeye detector, operating at 30 kV and 10 mA and using Cu Kα radiation (λ = 1.54184 Å). Diffraction data were collected over the 6°–60° 2θ range, with scan step 0.02° and counting time 60s per step. The identification of the crystalline phases in the XRPD patterns was carried out through the EVA-Bruker software (Bruker AXS, Karlsruhe, Germany), using the PDF2-2023 database (Gates-Rector and Blanton, 2019).

Transmission electron microscopy (HR-TEM), dark-field scanning-transmission electron microscopy (DF-STEM), energy-dispersive X-ray spectroscopy (EDS) and electron diffraction experiments on coatings were performed with a JEOL JEM-F2000 Multipurpose, working at 200 kV and equipped with Schottky-FEG source. EDS point analyses and elemental maps were performed with a JEOL SDD detector and quantified by the JEOL software.

X-ray absorption spectroscopy (XAS) analyses were performed at the X-ray fluorescence beamline (Karydas et al., 2018) of Elettra synchrotron (Trieste, Italy). XANES spectra were collected at room temperature using a Si(111) monochromator, with standard 45°/45° geometry for both transmission and fluorescence mode measurements, using an Hamamatsu Si-photodiode S3590-09, 10 × 10 mm^2, 300 µm thickness and an XFlash 5030 SDD detector (Bruker, Berlin, Germany), respectively. Pellet samples preparation procedure and additional beamline setup details are reported in Ghezzi et al., (2023). The average Cr oxidation state was determined using the least-squares Linear Combination Fitting (LCF) based on reference spectra of Cr-bearing compounds with known oxidation state and coordination geometry. Background removal, normalization of XANES spectra and LCF analyses (conducted in the energy range − 20 to 30 eV with respect to the absorption edge) were performed using the Athena software package (Ravel et al., 2005).

3.2. Water sampling and analysis

Groundwater from the deeper aquifer was sampled through a set of 10 m depth-specific piezometers (Fig. 2) during surveys on May 16, 2022 (dry season; samples PZ1-1, PZ3-1, PZ4-1 and PZ-5-1) and October 21, 2022 (wet season; samples PZ1-2, PZ3-2, PZ-5-2). Groundwater from the shallower aquifer was collected through a 2 m depth-integrated piezometer on May 16, 2022 (sample PZ2-1). Before sampling, three well-casing water column volumes were purged using a low-flow submersible pump. Electric conductivity, pH and redox conditions were continuously monitored during purging using a multiparameter probe (Hanna HI98195).

Waters from the surface runoff drainage system (samples VAS1 to VAS18, Fig. 2) were collected at open storage tanks (800 × 1200 mm in size) in different surveys on September 16, 2022; October 12, 2022; October 21, 2022; November 30, 2022, and June 15, 2023. It has to be noted that some of the tanks were empty prior to the arrival of a rain event, and not all the stations of the network were sampled in all the surveys.

Water samples were filtered in the field to 0.45 µm and stabilized using ultrapure HNO_3 for major cations and trace element analyses, stored in clean polyethylene vials and kept refrigerated until laboratory analysis. Temperature (T, °C), pH, and electrical conductivity (EC, µS/cm at 25 °C) were measured in the field using a digital thermometer and a pH/conductivity meter (Delta Ohm HD 2105.1). Uncertainties are ±0.8 °C, ±0.02 pH unit and ±0.5% µS/cm, respectively.

Alkalinity (totally expressed as bicarbonate ion) was determined in

Table 5
Soil leaching tests.

		C1-L	C2-L	C3-L	C4-L	C5-L	C6-L	C7-L	C8-L	C9-L	C10-L	C11-L	C12-L	C13-L	C14-L	C15-L	C16-L	C17-L
EC	µS/cm	242	1474	423	665	663	845	165	1158	2493	1175	923	822	1429	1453	1336	189	932
F	µg/l	660	570	310	430	550	390	390	310	660	380	450	610	300	340	230	1500	530
SO_4	mg/l	130	81.7	26.4	69.3	269	65.8	66.2	200	26.4	36.3	637	766	859	652	1096	68.8	411
Cl	mg/l	16.6	13.6	16.2	21.8	23.5	21.3	18.8	99.6	89.1	16.7	82.4	44.8	116	165	106	12.4	99.8
Ba	µg/l	20	12	64	23	27	46	42	18	84	67	29	58	33	36	28	17	35
Cu	µg/l	30	41	105	50	16	42	66	36	69	78	2.1	13	<1	<1	1.5	8.6	2.1
Zn	µg/l	<1	<1	<1	<1	<1	<1	1.1	<1	1.4	<1	<1	<1	1	<1	<1	<1	1.3
Be	µg/l	<0.05	<0.05	<0.05	<0.05	0.05	<0.05	<0.05	<0.05	<0.05	<0.05	<0.05	0.05	<0.05	<0.05	<0.05	<0.05	<0.05
Co	µg/l	1	3.4	4.7	2.2	<1	2.1	1.6	1	2.2	22.9	<1	<1	<1	<1	<1	<1	<1
Ni	µg/l	6.1	12	36	17	3.2	19	23	6.5	22	36	1.2	2.8	1	<1	<1	1.8	<1
V	µg/l	55	54	4.4	30	32	13	15	30	1.9	7.5	8.2	12	1.3	1.7	1.1	14	11
As	µg/l	4.4	4.5	1	3.3	4	2.1	2.1	2.1	<1	1.9	2	6.1	1.2	1	<1	6	2.3
Cd	µg/l	<0.05	<0.05	<0.05	<0.05	0.05	0.06	<0.05	<0.05	<0.05	<0.05	<0.05	0.07	<0.05	0.11	<0.05	<0.05	<0.05
Cr(VI)	µg/l	6.2	7.4	4.8	4.9	40	6.5	3.4	9	25	2.9	2.4	1.9	40	18	1.2	24	4.2
Pb	µg/l	<1	<1	1	<1	1	<1	<1	<1	2.4	<1	<1	<1	<1	<1	<1	<1	<1
Se	µg/l	2.3	4.5	1.1	3.6	10	3	2.2	3.2	1.2	6	3.5	26	13	7.1	1.2	1.4	1.8
Hg	µg/l	<0.1	<0.1	<0.1	<0.1	<0.1	<0.1	<0.1	<0.1	<0.1	<0.1	0.1	<0.1	<0.1	<0.1	<0.1	<0.1	0.1
Sb	µg/l	5.3	<1	2.8	3.3	5.5	1.8	<1	6.1	1.4	2.3	8.7	6.2	5.7	5.9	6.1	6.1	7.7

the laboratory by acidimetric titration. Major cations and anions were measured by ion-chromatography using a Thermo Fisher ICS-900 instrument. RSD was less than 5%. Trace elements were determined by ICP-MS using a Perkin Elmer NexIon 300X. A blank solution was run every ten samples. Reference solutions NIST SRM 1640a and 1643f were analyzed together with the water samples. Precision was better that 10 % RSD. Deviations from the certified standard values were less than 5%, except for As, Ba, Cu, Fe, Li, V (5–10%) and Zn (10–12%). The detection limit was calculated as the mean value of the sum of the blank solution concentration (20 replicates) and three times the standard deviation. It was: 0.007 µg/L (Be, Cd, Co, Tl), 0.005 µg/L (Th, U), 0.02 µg/L (As, Sb, Sn), 0.08 µg/L (Li, Cr, Pb, V), 0.04 µg/L (Ag), 0.1 µg/L (Ni, Mo), 0.4 µg/L (Ba, Cu, Mn, Sr), 2 µg/L (Fe), 4 µg/L (Zn).

Hexavalent chromium was determined using a Dionex DX-500 ion chromatography system with an AD-20 UV–Vis absorbance detector. A Hamilton PRP-X-100 analytical column (4 × 250 mm, 5 µm particle size) was used for separation. After elution, a Cr(VI)-complex was formed by post-column derivatization reaction with DPC through a 750 µl knitted reaction coil. The detection limit was 0.2 ppb.

Cr-isotopes were determined on unacidified water samples after filtration in the field. Sample preparation was performed in a Class 10000 clean lab to prevent contamination (ALS Scandinavia AB). Water samples were evaporated to dryness at 80 °C on hot plate. Solid residue was digested by 5 ml aqua regia and evaporated to dryness, followed by dissolution in 4 ml HCl 0.2 M and column Cr separation using a DOWEX AG 1 × 8 anion exchange resin. Purified fractions were spiked with internal standard (Ni); the $^{53}Cr/^{52}Cr$ ratio was measured by MC-ICP-MS (Neptune PLUS, Thermo Scientific, Bremen, Germany) using a combination of internal standardization and external calibration (Pontér et al. (2016). Due to the lack of accredited water Cr-isotope standard, Milli-Q water spiked with Cr standard was subjected to the same water sample preparation routine. Acceptance criterion is that $\delta^{53}Cr$ for purified Cr does not differ from value before purification by more than 1 per mill. Recovery after column chemistry must be better that 90%. The measured $^{53}Cr/^{52}Cr$ ratios were expressed using the conventional δ-notation referred to the NIST SRM 979 standard:

$$\delta^{53}Cr = [(^{53}Cr/^{52}Cr_{sample}/^{53}Cr/^{52}Cr_{SRM979})\text{-}1]x1000 \quad (1)$$

4. Exposure models and risk assessment

The maximum allowed concentration of contaminants in soil, considered to be protective of human health (soil screening levels—SSLs, according to US EPA guidelines), for total and hexavalent chromium was obtained by following the Risk Based Corrective Action procedure, which applies the deterministic approach outlined in ASTM standards (ASTM, 2000) and United States Environmental Protection Agency (US EPA) guidelines (US EPA, 1996, 2002, 2023a). The selected exposure routes were surface soil ingestion, dermal contact and soil dust inhalation, typical for a residential setting. In this approach, the exposure equations and pathway models used for estimating the potential adverse effects on receptors (e.g. US UT, 2023) are run in reverse to back-calculate the acceptable level of contaminant concentration in soil corresponding to the target risk (US EPA 2023b). Risk-based SSLs for the different outdoor exposure pathways and for residential settings were derived from standardized sets of equations (US EPA, 2002, 2023b) using the Risk-net software (version 3.1.1 pro).

The equation related to the carcinogenic effect for hexavalent chromium (modified after US EPA Guidelines) are:

$$SSL_{ing} = \frac{TR_{ing} \text{ x } AT}{SF_{oral} \text{ x } 10^{-6}\left(\frac{kg}{mg}\right) \text{ x } RBA \text{ x } EF \text{ x } ADJ_{ing}}$$

$$SSL_{derm} = \frac{TR_{derm} \text{ x } AT}{SF_{derm} \text{x } 10^{-6} \left(\frac{kg}{mg}\right) \text{x } EF \text{ x } ABS \text{ x } ADJ_{derm}}$$

$$SSL_{inhal} = \frac{TR_{inhal} \text{ x } AT}{IUR \text{ x } 10^{3} \left(\frac{\mu g}{mg}\right) \text{ x } EF \text{ x } ET \text{ x VFp x } (ED_c \text{ x } ADAF_{0-6} + ED_a \text{ x } ADAF_{6-30})}$$

where:

$$ADJ_{ing} = \frac{ED_c \text{ x } IR_{ing-c} \text{ x } ADAF_{0-6}}{BW_c} + \frac{ED_a \text{ x } IR_{ing-a} \text{ x } ADAF_{6-30}}{BW_a}$$

$$ADJ_{derm} = \frac{ED_c \text{ x } SA_c \text{ x } SAF_c \text{ x } ADAF_{0-6}}{BW_c} + \frac{ED_a \text{ x } SA_a \text{ x } SAF_a \text{ x } ADAF_{6-30}}{BW_a}$$

with TR_{ing} the total carcinogenic risk for a single substance, represented by the sum of the contributions due to each exposure route, set to 10^{-6} (US EPA 1996, 2002). The toxicity reference value for direct exposures and carcinogenic effect is represented by the slope factor (SF) which converts the estimated daily intake averaged over a lifetime of exposure directly into the incremental risk for an individual to develop cancer. For the dermal pathway, SF_{derm} was derived from SF_{oral} applying the "GIABS" factor (which represents the fraction of contaminant absorbed in the gastrointestinal tract in the critical toxicity study; US EPA, 2004). In the case of the dust inhalation pathway (US EPA, 2009), the Inhalation Unit Risk (IUR), defined as an estimate of the increased cancer risk from inhalation exposure to a given concentration in air (1 μg/m^3) for a lifetime, was used. Inhalation of contaminants adsorbed on breathable particles due to wind erosion was assessed using a generic VFp factor (Cowherd et al., 1985) equal to 6.90×10^{-12} kg/m^3, calculated using the default values suggested by ASTM (ASTM, 2000).

The Risk-based SSLs for carcinogenic risk due to direct exposure (ingestion and dermal contact) was calculated using an age-adjusted factor (ADJ), namely a time-weighted average of age-dependent parameters for receptors exposed for an extended time from childhood through adulthood (US EPA, 2002, 2023b). Furthermore, since Cr (VI) is carcinogenic by a mutagenic mode of action, the Age-Dependent Adjustment Factor (ADAF) was also applied when assessing cancer risks from early-life exposure. The recommended values are reported in Table 1. Similar standardized sets of equations, based on the updated U. S. Environmental Protection Agency's human health risk assessment methods, can provide soil screening levels even in the case of non-carcinogenic effect for children and adults respectively. For non-carcinogenic effects, the contaminant specific toxicity reference dose (RfD, mg/kg/day), defined as the maximum daily exposure to a toxic agent that would not produce any appreciable deleterious effect on human health, was applied. In the case of inhalation pathways the Reference Concentration (RfC, mg/m^3) replaces the Inhalation Unit Risk (IUR; US EPA, 2009).

5. Results

5.1. Geochemical characterization of solid materials

The geochemical characterization of KEU-bearing aggregate is reported in Table 2. The total chromium content (Cr_{tot}) is in the range between 3388 and 8384 mg/kg, and Cr(VI) between 4.7 and 22 mg/kg, above the concentration thresholds for soil in residential areas imposed by Italian regulations (150 mg/kg and 2 mg/kg for Cr_{tot} and Cr(VI) respectively). In addition, all samples exceed the maximum allowable concentration for Cr(VI) established by the Italian regulation for end-of-waste criteria (2 mg/kg). Samples P3 and P5 exceed the concentration limit for Cd (2 mg/kg); samples P1, P2 and P3 exceed the limit for Co (2 mg/kg); samples P3, P4, P5 and P7 exceed the maximum permitted concentration for Pb (100 mg/kg); samples P1, P3, P5 and P6 for Se (3 mg/kg). The data indicate that, besides Cr, the KEU-bearing aggregate material contains a number of potentially toxic chemicals.

The results of the geochemical analysis on soil are reported in Table 3. The Cr_{tot} concentration values lie in the wide range between 72 and 4170 mg/kg, in some cases largely exceeding the concentration threshold for soil in residential settings (150 mg/kg). Hexavalent chromium ranges between 0.92 and 31 mg/kg, in most cases above the 2 mg/kg guideline for residential settings. Nickel, Cu, Zn, Co, Sb and Se also exceed the concentration limits (120 mg/kg; 120 mg/kg; 150 mg/kg 20 mg/kg; 10 mg/kg and 3 mg/kg, respectively) in some of the samples.

5.2. Leaching tests

The geochemistry of leachates from the KEU-bearing aggregate is given in Table 4. Chromium is totally in its hexavalent form, ranging between 390 and 1880 μg/L, i.e., well above the maximum permissible limit for Cr(VI) in groundwater (5 μg/L) and the threshold for Cr_{tot} in end-of-waste solutions (50 μg/L). In addition, Sb exceeds the 5 μg/L limit for groundwater. It is also worthy of note that leachates are enriched in sulfate ions, ranging between 535 and 1229 mg/L, exceeding by far the regulatory limit of 250 mg/L.

The results of leaching tests on soil samples are reported in Table 5. The total amount of Cr

Measured in leachates is Cr(VI), ranging between 1.2 and 40 μg/L. In particular, samples C1-L, C2-L, C5-L, C6-L, C8-L, C9-L, C13-L, C14-L, C16-L exceed the Cr(VI) concentration limit of 5 μg/L. In addition, samples C3-L, C7-L, C9-L, C10-L have Ni concentration in the range between 22 and 36 μg/L, above the 20 μg/L threshold for groundwater. The Sb concentration ranges from below the detection limit (<1 μg/L) to 8.7 μg/L. In particular, the Sb content in samples C1-L, C5-L, C8-L and samples C11-L to C17-L is above the 5 μg/L target for groundwater quality. Leachates are also characterized by highly variable sulfate (between 26.4 and 1096 mg/L) and fluoride (in the range between 310 and 1500 μg/L) content.

The Cr(VI) concentration in the leaching solution in contact with coatings on roadway gravel was 2300 and 4050 μg/L after 48 h and 7 days, respectively, indicating that coatings contain hexavalent chromium which is easily released to water.

5.3. Mineralogy

X-ray diffraction analysis indicates that coatings are made of gypsum, calcite, portlandite ($CaO \cdot H_2O$), thenardite (Na_2SO_4) and rare iron oxyhydroxides. TEM-EDS analyses revealed the occurrence of calcium carbonates and calcium sulphates, in addition to rare silicates and a phase highly enriched in Cr. The latter typically appears as grains of few hundreds nanometers, with sub-euhedral margins (Fig. 3). The main constituents, in descending wt% abundance order, are oxygen, silicon, chromium, magnesium, calcium and sulfur (Table 6). Grains of the Cr-rich phase show a significant fluctuation in composition, but the ranking among the cations remains fairly constant, and, in particular, Cr

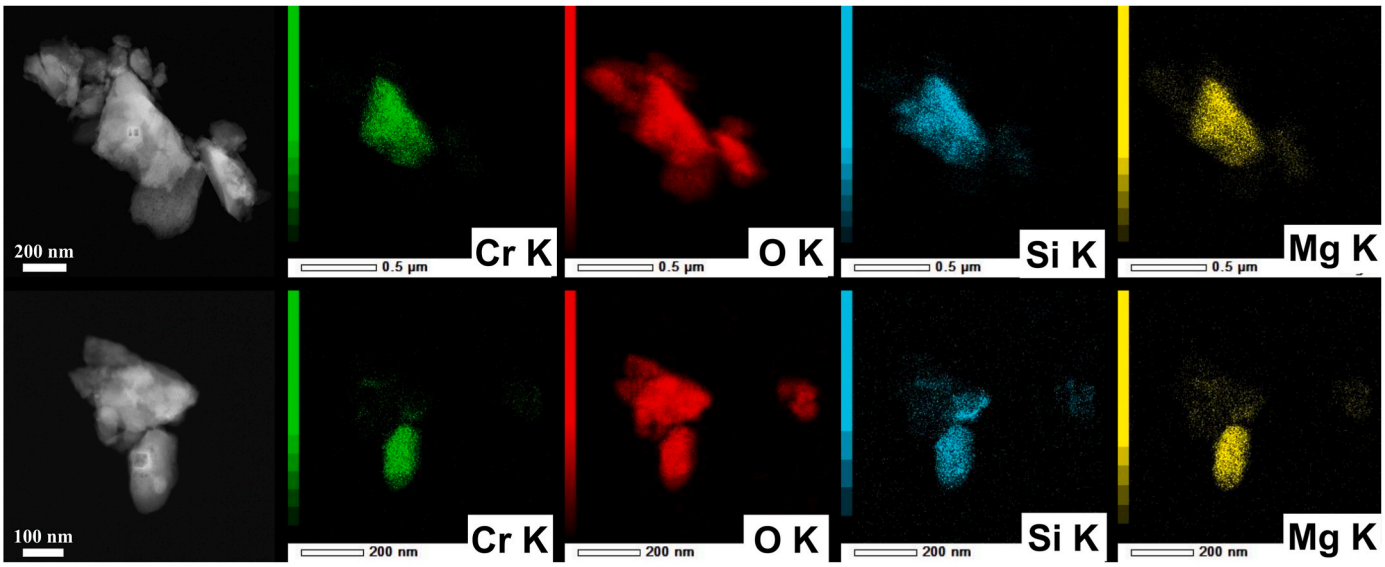

Fig. 3. Dark-field STEM images of two Cr-rich grains in coatings, scratched from gravels in unpaved roads, and related EDS maps for Cr, O, Si and Mg. The beam damage produced by EDS analysis is clearly evident in the STEM images in the shape of etched squares.

Table 6
TEM-EDS quantification for four Cr-grains scratched from the green halo (wt%).

	#1	#2	#3	#4	AVERAGE
O	44.67	56.40	52.72	51.94	51.44
Mg	9.14	4.63	8.08	5.83	6.92
Si	11.06	14.82	9.45	14.87	12.55
S	3.50	1.37	3.62	1.64	2.53
Ca	4.96	4.62	4.60	5.66	4.96
Cr	26.67	18.16	21.53	20.06	21.60

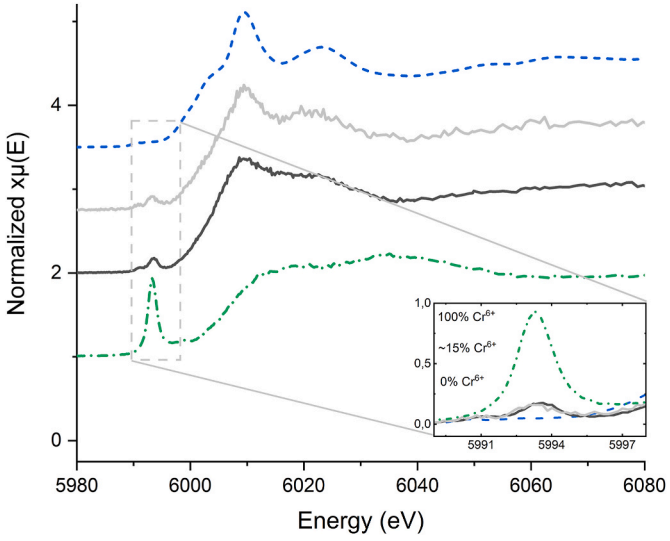

Fig. 4. Normalized XANES spectra representative of coatings (grey and black lines, respectively) together with those of reference compounds chromite (Cr^{3+}) and crocoite (Cr^{6+}) (dashed and dash-dotted lines, respectively) collected at the Cr K-edge. The small box on the bottom right is a zoom around the pre-edge peak area, to better highlight the presence (and same intensity) of the typical Cr^{6+} peak in both coating samples.

is always the most abundant cation, with about 22 wt% (about 44 at% when only cations are considered). Despite the apparent euhedral shape of the Cr-rich grains, electron diffraction reveals that they are completely amorphous.

The XANES spectra of the Cr-bearing coatings indicate the presence of Cr(III), likely in octahedral coordination, and of about 15% Cr(VI), as witnessed by the typical pre-edge peak for Cr(VI) at about 5993.0 eV (Fig. 4).

5.4. Water

The physico-chemical parameters and major ion chemistry of groundwater collected by the piezometers are reported in Table 7. Groundwater temperature ranges between 14.2 and 19.4 °C; pH ranges between 6.7 and 7.1, and dissolved oxygen (DO) is between 1.2 and 4.0 mg/L, indicating changes in the oxygen consumption rate. Electrical conductivity (EC) varies between 1142 and 2830 μS/cm (TDS between 1208 and 2878 mg/kg), the highest EC being measured in the shallower PZ2 piezometer.

The data obtained for surface water collected from the drainage system are also reported in Table 7. For these samples, the temperature ranges between 13.0 and 20.1 °C; pH and DO are highly variable at a different spatial scale, ranging between 7.5-9.2 and 0.8–14.8 mg/L, respectively. Dissolved oxygen and pH are both elevated in VAS3 and VAS6 stations, suggesting the possible role of algal photosynthesis in open tanks during the day, consuming CO_2 and causing pH and O_2 concentration to rise. In the Piper diagram (Fig. 5) groundwater belongs to the Ca–HCO_3 water type. A relative SO_4^{2-} enrichment is observed in the PZ2-1 sample, draining the shallower aquifer, and belonging to the Ca–SO_4 water type. Surface waters from the runoff drainage system range from the Ca–HCO_3 to the Na–Ca–SO_4 type.

Silica in groundwater and surface water ranges between 9 and 21 mg/L and between 8 and 60 mg/L, respectively. The relatively high silica content might reflect the release from KEU (average Si content 2.8 wt%) or their active degradation of silicate mineral phases. The latter hypothesis is supported by the water chemistry, which is consistent with kaolinite formation in the silicate system.

The trace element concentration measured in groundwater and surface water are reported in Table 8. The Cr(VI) content in groundwater and the Cr(VI) and $\delta^{53}Cr$ values in surface water are given in Table 9. It must be noted that, within experimental uncertainty, chromium in both surface and shallow ground water is totally in the hexavalent form. Groundwater is characterized by relatively high Mn, and, in some samples, high Fe and Ni, with values above the maximum concentration levels admitted by Italian regulations (50, 200 and 20 μg/L for Mn, Fe

Table 7
Physico-chemical parameters and major ion chemistry of groundwater (PZ samples) and surface water (VAS samples).

	T (°C)	DO (mg/L)	pH	EC (μS/cm)	Na^+ (mg/L)	K^+ (mg/L)	Mg^{2+} (mg/L)	Ca^{2+} (mg/L)	Cl^- (mg/L)	NO_3^- (mg/L)	SO_4^{2-} (mg/L)	HCO_3^- (mg/L)	SiO_2 (mg/L)
May 16, 2022													
PZ1-1	14.2	1.74	6.8	1299	140	4.7	65.9	182	112	nd	377	557	9.0
PZ2-1	17.8	3	6.7	2830	311	11.5	72	491	447	nd	984	643	21.0
PZ3-1	17.3	3.25	6.9	1807	166	1.1	82.1	248	254	nd	387	675	15.2
PZ4-1	14.4	1.2	6.9	1142	96.0	1.7	60.2	159	129	nd	13.4	806	16.2
PZ5-1	17	1.22	6.8	1582	76.1	2.0	40.5	234	158	nd	229	572	14.8
October 21, 2022													
PZ1-2	19.4	4	7.1	1839	137	9.1	63.0	146	109	nd	363	476	12.6
PZ3-2	17.8	3.2	6.9	1708	107	1.00	52.6	158	175	nd	298	629	16.2
PZ5-2	17.7	2.7	7	1462	68.8	0.97	40.5	235	154	nd	259	525	14.8
October 21, 2022													
VAS1	17.8	6.2	7.9	884	86.9	31.5	12.8	70.7	45.3	9.8	279	171	20.6
VAS2	17.3	5.2	7.8	776	56.7	43.7	11.6	83.2	88.2	nd	7.6	348	8.4
VAS3	18.3	14.8	9.2	2170	130.0	40.9	30.8	267	78.3	185	932	79	22.0
VAS4	18.4	7.0	7.6	1024	88.3	32.5	12.7	90.1	47.4	3.7	327	98	16.4
VAS5	13	0.8	7.8	836	19.3	54.8	13.0	88.1	50.9	nd	17.3	494	60.0
VAS6	16.8	12.6	8.6	593	32.5	43.2	12.6	67.1	39.8	nd	65.0	293	24.0
VAS7	16.8	1.2	7.8	836	35.7	54.6	16.7	63.1	52.0	nd	2.3	378	43.6
VAS8	20.1	3.9	7.5	800	58.9	6.2	21.2	84.1	55.7	3.4	61.2	372	23.6

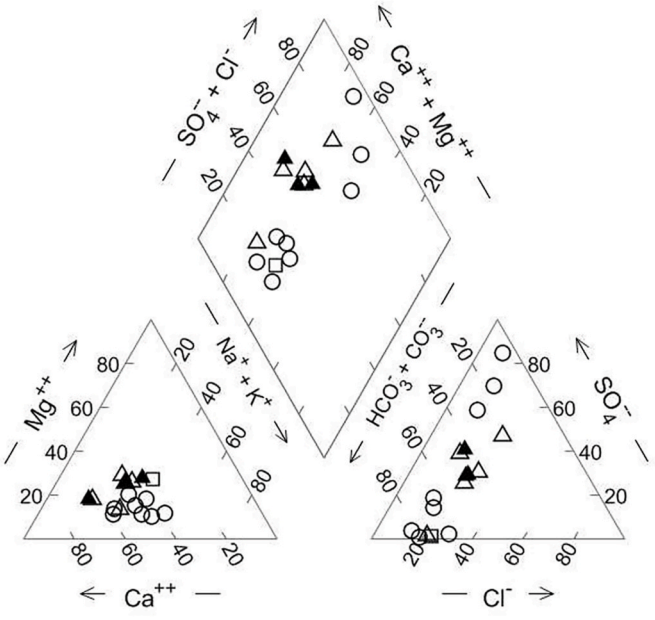

Fig. 5. Piper diagram. Symbols are: solid and open triangle, water collected from piezometers on May 15 and October 21, 2022, respectively; open circle, surface water from the drainage system collected on October 21, 2022.

and Ni, respectively). Relatively high concentrations of Mn, Fe and Ni are commonly found in groundwater from aquifers in the Arno and Serchio river alluvial plain, and they are attributed to geogenic sources. In particular, the highest Fe concentration is observed in the PZ4 and PZ5 piezometers, which sample the most reducing portions of the aquifer. Arsenic in PZ4-1 exceeds the 10 μg/L limit imposed by Italian regulations, possibly reflecting the release of As hosted in sulfide minerals that characterize the outcrops in the Arno and Serchio river catchment areas. The groundwater sample PZ2-1, from the shallower aquifer, and some surface water samples from the runoff receptor system are characterized by Sb concentrations above the maximum admissible limit of 5 μg/L. Antimony is not attributable to geogenic sources, and was likely mobilized from the KEU-bearing aggregate. It is worth to note that groundwater from the deeper aquifer shows very low Cr(VI) concentration; on the contrary, surface water shows highly variable Cr(VI) content (Fig. 6), reaching 18000 μg/L in VAS10 on November 30, 2022. These data confirm the occurrence of a Cr(VI) leaching flux and dispersion on the soil surface via aqueous routes. On the other hand, at present, the data do not indicate any contamination for the deeper groundwater exploited for drinking purposes.

Chromium in the KEU source has $\delta^{53}Cr$ value close to 0‰ relative to NIST 979 (average $\delta^{53}Cr = -0.031 \pm 0.057$). The $\delta^{53}Cr$ in surface water ranges between $+1.581 \pm 0.038$ ‰ and $+3.261 \pm 0.191$ ‰ (Fig. 7). Positive $\delta^{53}Cr$ values reflect the different extent of reduction at each station, which is not constant over time. Indeed, the reduction of Cr(VI) causes a significant $^{53}Cr/^{52}Cr$ shift due to isotopic fractionation, resulting in the enrichment of ^{53}Cr relative to ^{52}Cr in the remaining Cr (VI) pool, thus yielding positive $\delta^{53}Cr$ values (Ellis et al., 2002).

5.5. Risk analysis

The calculated individual soil screening levels (SSLs) are reported in Table 10. It can be observed that the screening value for Cr(VI) for a residential setting (0.156 mg/kg), taking into account the carcinogenic effect, is much lower compared with the Cr(VI) concentration measured in soil (Table 3) and even significantly lower than the threshold imposed by Italian regulations for residential soil (2 mg/kg). The SSLs for Cr_{tot}, intended as non-carcinogenic Cr(III), are well above the Cr_{tot} concentration values measured for all the exposure pathways.

6. Discussion

The geochemical data highlight that Cr represents the main environmental concern at Green Park. A relatively high total Cr content characterizes the natural sediments in the alluvial plain of the Arno and Serchio rivers where Green Park is located; these sediments originated

Table 8
Concentration of trace elements considered (μg/L) in groundwater (PZ samples) and surface water (VAS samples) together with the maximum concentration level (MCL, μg/L) imposed by Italian regulations for groundwater. Values in bold exceed the MCL.

	Li	Be	Mn	Co	Ni	Cu	Zn	Sr	Mo	Ag	Sn	Cd	Sb	Ba	Tl	Pb	Th	U	V	Fe	As
MCL		4	50	50	20	1000	3000			10		5	5		2	10				200	10
May 16, 2022																					
PZ1-1	2.67	<0.06	**237**	0.37	11.1	4.3	<42	1066	<1.5	<0.2	<0.25	<0.1	<0.3	61	<0.1	<0.5	<0.1	3.82	<0.6	24	0.27
PZ2-1	5.30	<0.06	**327**	3.4	**48**	13.2	120	1716	7.56	0.15	<0.25	0.36	2.21	52	0.06	<0.5	<0.04	7.3	1.06	35	0.25
PZ3-1	3.18	<0.06	**138**	0.53	17.7	4.5	<25	1212	<0.9	0.34	<0.25	<0.1	0.26	83	0.08	<0.5	<0.04	3.55	0.68	7.8	0.72
PZ4-1	1.70	<0.06	**822**	1.14	**20.2**	3.22	25	1205	2.01	0.16	<0.25	<0.1	0.35	508	0.06	<0.5	<0.04	0.84	1.03	**11078**	**33**
PZ5-1	1.45	<0.06	**1687**	1.78	12.5	1.87	<25	823	<0.9	<0.12	<0.25	<0.1	<0.2	552	0.06	<0.5	<0.04	0.29	<0.34	**3805**	0.19
October 21, 2022																					
PZ1-2	4.2	<0.06	**110**	0.24	6.9	6.3	<25	1164	<0.9	0.36	0.20	<0.04	0.26	42	0.14	<0.32	<0.04	2.60	<0.34	<21	<0.1
PZ3-2	5.8	<0.06	**1889**	0.67	21	5.5	<25	1280	<0.9	<0.12	<0.15	<0.04	<0.2	68	<0.06	1.01	<0.04	2.33	0.41	<21	0.45
PZ5-2	2.8	<0.06	**2709**	1.70	9.8	2.9	<13	1062	0.63	<0.06	<0.08	<0.02	<0.1	556	<0.03	<0.16	<0.02	0.35	<0.17	**6951**	0.68
September 16, 2022																					
VAS1	13.3	0.03	2.20	0.33	2.94	7.4	<16	446	21.0	0.45	<0.1	<0.03	**6.6**	40	0.08	<0.2	<0.03	1.69	6.6	<14	0.77
VAS2	8.3	0.03	**619**	1.09	8.1	4.0	<16	597	5.5	0.46	<0.1	<0.03	0.76	136	<0.04	0.94	0.09	0.46	2.66	**1118**	**13.6**
VAS3	33	0.02	2.98	0.77	7.3	12.9	<16	1132	24.4	0.43	<0.1	<0.03	15.2	58	0.07	<0.2	<0.03	1.17	6.6	<14	1.14
VAS4	17.4	0.02	5.5	0.36	4.5	7.3	<16	846	17.2	0.32	<0.1	<0.03	4.7	75	0.06	<0.2	<0.03	0.87	2.34	<14	1.37
October 12, 2022																					
VAS1	15.9	<0.07	6.1	0.32	3.2	6.8	<17	444	19.1	<0.25	<0.3	<0.03	**6.2**	60	<0.04	<0.2	<0.03	1.41	5.4	<14	0.71
VAS2	8.6	<0.07	**232**	0.74	6.5	2.6	<17	465	4.7	<0.25	<0.3	<0.03	0.70	126	<0.04	0.34	0.08	0.50	1.77	**535**	5.5
VAS3	42	<0.07	9.7	1.03	9.9	11.5	<50	1320	22	<0.25	<0.3	<0.09	**16.3**	71	<0.11	<0.6	<0.08	1.57	4.8	<35	1.24
VAS4	19.8	<0.07	2.5	0.38	5.0	7.3	<17	929	20	<0.25	<0.3	<0.03	**5.4**	75	<0.04	<0.2	<0.03	1.06	1.69	<14	0.64
October 21, 2022																					
VAS1	15.4	<0.06	16.6	0.33	3.0	6.6	<13	453	18.9	<0.06	<0.08	<0.02	**6.2**	62	<0.03	<0.16	<0.02	1.45	6.2	<11	0.96
VAS2	8.7	<0.06	126	0.71	6.3	2.1	<13	483	5.2	<0.06	<0.08	<0.02	0.64	118	<0.03	<0.16	<0.02	0.64	1.54	121	4.28
VAS3	46	<0.06	8.0	1.09	10.6	16.5	<42	1515	28	<0.2	<0.3	<0.1	**16.0**	71	<0.1	<0.5	<0.1	0.97	4.8	<35	0.78
VAS5	16.2	<0.06	**863**	1.30	5.4	1.2	<13	634	0.19	<0.06	<0.08	<0.02	0.45	96	<0.03	<0.16	<0.02	0.16	1.20	**267**	2.68
VAS6	15.4	<0.06	**277**	0.63	7.3	<1.7	<25	396	10.8	<0.12	<0.15	<0.04	1.05	97	<0.06	<0.32	<0.04	1.45	2.35	43	2.85
VAS7	13.3	<0.06	**362**	0.39	3.4	1.7	<13	259	0.52	<0.06	<0.08	<0.02	0.66	28	<0.03	<0.16	<0.02	0.05	0.77	**327**	2.47
VAS8	9.3	<0.06	6.8	0.15	2.4	2.5	<13	411	4.1	<0.06	<0.08	<0.02	1.27	129	<0.03	<0.16	<0.02	0.27	1.48	<11	0.37

Table 9
Cr(VI) concentration and δ^{53}Cr isotopic values (‰). Errors on δ^{53}Cr values are reported at 95% confidence level.

	Cr(VI)(μg/L)	δ^{53}Cr	err
May 16, 2022			
PZ1-1	0.50		
PZ2-1	165		
PZ3-1	0.09		
September 16, 2022			
VAS1	980	2.332	0.146
VAS2	2.0		
VAS3	6929	2.261	0.083
VAS4	67	3.261	0.191
October 12, 2022			
VAS1	640		
VAS2	8.9		
VAS3	6844	2.572	0.061
VAS4	228		
October 21, 2022			
VAS1	548	2.509	0.068
VAS2	1.30		
VAS3	6487	2.663	0.07
VAS5	0.60		
VAS6	0.40		
VAS7	0.40	2.117	0.228
VAS8	161	2.176	0.09
November 30, 2022			
VAS1	430	2.306	0.068
VAS3	3500	1.923	0.056
VAS4	300		
VAS8	820		
VAS9	680	2.123	0.044
VAS10	18000	1.581	0.038
VAS11	100		
VAS12	3600		
VAS13	15000		
VAS14	3200		
VAS15	1200		
VAS16	890		
VAS17	720		
VAS18	990		
June 15, 2023			
VAS1	80	3.085	0.427
VAS3	1650	1.977	0.091
VAS4	340	2.385	0.102
VAS8	490	2.397	0.111
VAS10	1000	1.905	0.067
VAS12	620		
VAS13	1860		

from the weathering and erosion of the ultramafic ophiolitic outcrops in the highland Apennine catchments (Dinelli et al., 2005). The vanadium content represents an ultramafic source-rock signature (Amorosi et al., 2013) reflecting the ophiolitic rocks petrogenesis (Shervais, 1982). Still, it can be observed that most soil samples at Green Park deviate towards nickel enrichments and, even more distinctly, towards chromium ones compared with the trend reported for natural soil and sediments in the plain (Fig. 8), suggesting a variable contribution from the KEU-bearing aggregate source.

Despite extraction experiments demonstrated that the just-produced KEU does not contain measurable amounts of hexavalent chromium, ageing experiments have shown that a time-dependent Cr(III)–Cr(VI) inter-conversion occurs when KEU remains exposed to air and moisture at ordinary ambient conditions (Ghezzi et al., 2023). This has been ascribed to the potential for trivalent chromium hosted in CrOOH oxy-hydroxides that characterize the KEU mineral assemblage to be oxidized to Cr(VI) (Liu et al., 2020). This process represents the crucial step that transforms KEU from an inert waste to a hazardous material, and implies that the KEU-bearing aggregate in the site Green park, represents a source for both Cr(III) and Cr(VI). The latter may be leached during rainfall events, migrates through water courses on the soil surface and enters the Green Park drainage system. The fate of Cr(VI) in the water-soil system primarily depends on adsorption/desorption

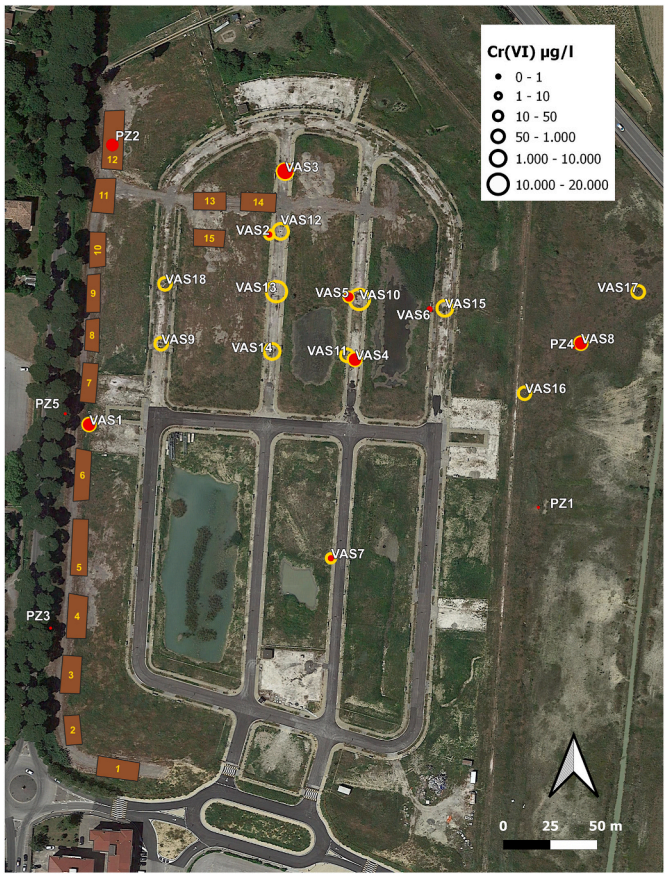

Fig. 6. Hexavalent chromium distribution in surface water from the drainage system during the dry (filled circles) and wet (open circles) seasons. The Cr(VI) concentration scale is shown.

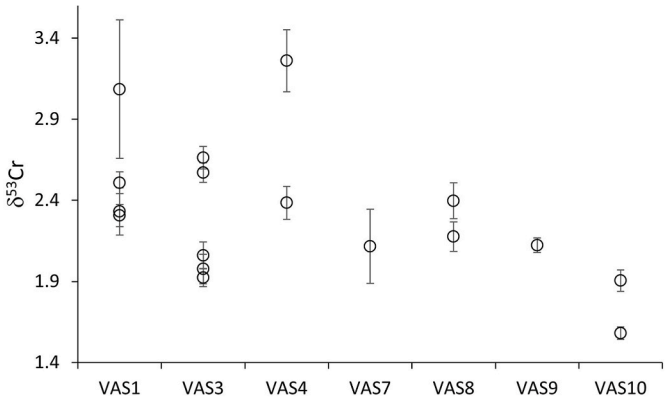

Fig. 7. Pattern of δ^{53}Cr values (‰) in surface water at the different sampling stations (VAS samples).

processes and on its decay by reduction to the trivalent form, which is readily immobilized in the soil matrix (Wittbrodt and Palmer, 1995; Khan et al., 2010; Jardine et al., 2013). Also hexavalent chromium oxy-compounds may have sorption affinity for some mineral surface, such as naturally occurring iron oxydrydroxides (Liu et al., 2021), remaining however relatively mobile to soil water (Fendorf et al., 1997). The hexavalent chromium contents measured in soil samples during the 2024 survey indicate that Cr(VI) was significantly retained by soil surface layers; in particular, the highest concentrations were observed near the KEU-bearing stockpiles, which represent the primary source of contamination, and the concentration decreased with increasing

Table 10
SSL (surface soil) calculated for each exposure route, for children (defined as an individual between one and six years of age) and adult receptors (in brackets values for adults when different). SSLs representative of the sum of all soil exposures were calculated according to (US EPA, 2023b). For Chromium (VI) only the most precautionary SSLs from carcinogenic effect are reported (represented by a single value because they were calculated using an age-adjusted factor, see text).

SSL	Soil Ingestion	Dermal Contact	Inhalation dust	Sum of soil exposures
Cr_{tot} (considered as non- carcinogenic Cr(III)) $RfD_{oral} = 1.5$ mg/kg/day (*) $RfD_{derm} = 1.95 x10^{-2}$ (***) $GIABS = 0.013$ (**) $RfC = 1.4x10^{-4}$ mg/m^3 (*)	1.17×10^5 (1.09×10^6)	5.45×10^4 (3.57×10^5)	8.82×10^5	0.36×10^5 (2.06×10^5)
Cr(VI) (carcinogenic) $SF_{oral} = 0.5$ (mg/kg/day)$^{-1}$ (**) $SF_{derm} = 20$ (***) $GIABS = 0.025$ (**) $IUR = 8.4x10^{-2}$ (μg/m^3)$^{-1}$ (**)	0.336	0.29	2.33×10^3	0.156

*US TCEQ (2023), **US EPA (2023a), *** RfD_{derm} and SF_{derm} are derived from RfD_{oral} and SF_{oral}, respectively, applying a gastrointestinal absorption factor (GIABS, unitless) to adjust (RfD_{derm} = RfD_{oral} x GIABS and $SF_{derm} = SF_{oral}/GIABS$) available oral toxicity values (US EPA2023a).

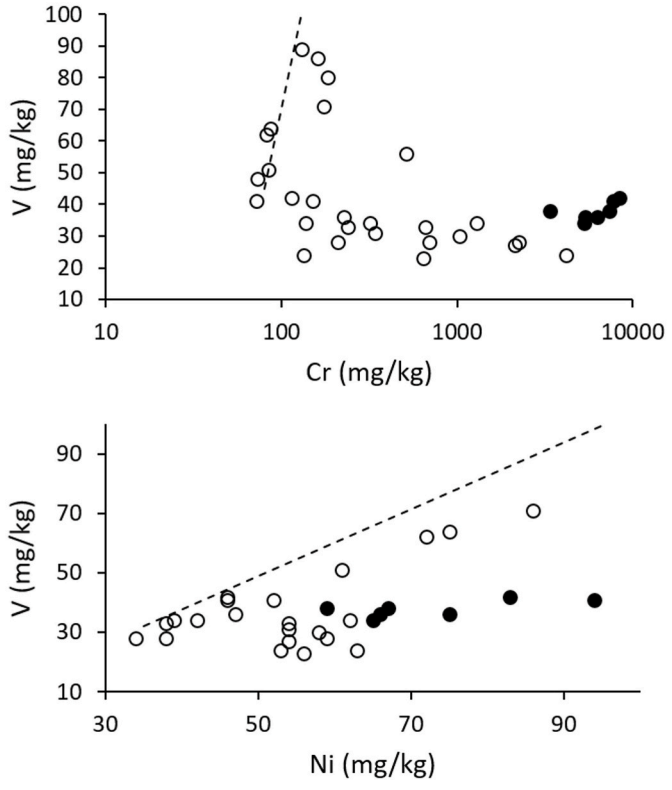

Fig. 8. Cr *vs* V and Ni *vs* V correlation diagrams. Symbols are: dots, KEU-bearing aggregate; open circles, soil. The correlation reported for the Arno and Serchio river alluvial plain sediments and attributed to geogenic sources is superimposed (Amorosi et al., 2013; dashed line).

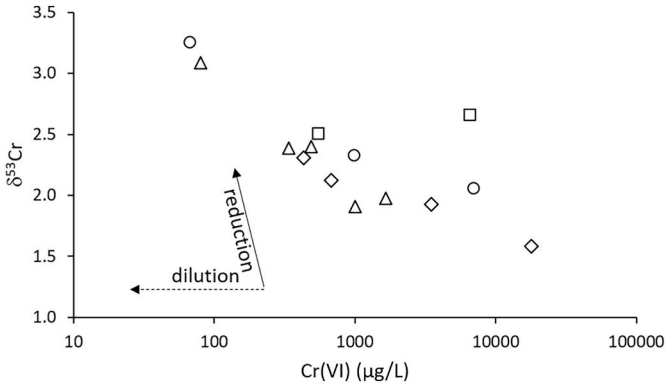

Fig. 9. Cr(VI) *vs* δ^{53}Cr correlation diagram for surface water. The effects of dilution, which leaves the δ^{53}Cr unchanged, and Cr(VI) reduction assuming a Rayleigh fractionation law (α = 0.9958; Kitchen et al., 2012) are shown. Symbols are: open circle, September 16, 2022; open square, October 21, 2011; open diamond, November 30, 2022; open triangle, June 15, 2023 surveys.

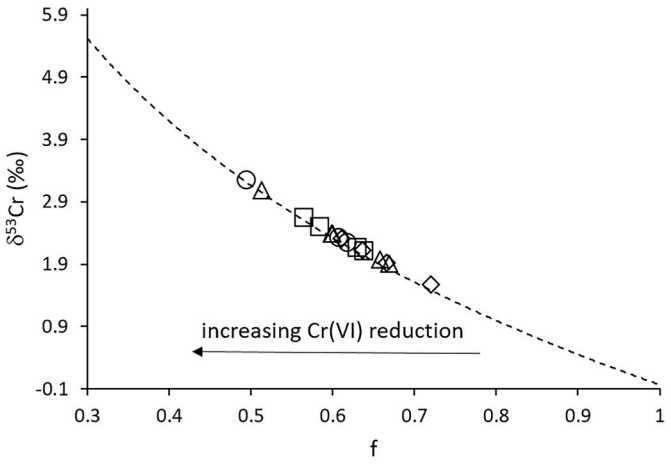

Fig. 10. Fraction of Cr(VI) remaining (f) *vs* δ^{53}Cr during progressive reduction, according to a Rayleigh fractionation model (α = 0.9958), for surface waters collected during different surveys and assuming the background Cr isotopic composition of KEU (δ^{53}Cr = −0.031). Symbols are: open circle, September 16, 2022 sampling; open square, October 21, 2022; open diamond, November 30, 2022; open triangle, June 15, 2023.

distance from the stockpiles.

The Green Park surface waters are invariably characterized by positive δ^{53}Cr, indicating that Cr(VI) underwent reduction during transport, after the initial mobilization from the KEU-bearing aggregate source. Cr-isotope data also suggest that the reduction processes have been variable at temporal and spatial scales. Hydrogen sulfide in the aqueous phase represents one of the strongest reducing agents for Cr(VI) (e.g. Kim et al., 2001); noteworthily, sulfate concentration in contaminated water at Green Park decreases as the amount of bicarbonate ions increases, yielding the observed shift parallel to the anion axis in the Piper diagram (Fig. 5); this suggests that sulfate reduction to hydrogen sulfide by organic matter is an active process. In addition to H_2S, Fe(II) in aqueous solution is an important reductant for Cr(VI) (Pettine et al., 1998), and iron oxy-hydroxides, ubiquitous in the plain, may promote chromate abiotic and biotic reduction in soil and water systems (e.g. Whitaker et al., 2018; Wielinga et al., 2001; Hu et al., 2021).

A rough increasing trend of δ^{53}Cr with decreasing Cr(VI) concentration in surface water is observed (Fig. 9). This pattern likely reflects the complex relationship between the action of different reductants and dilution processes by rainwater. Assuming a Rayleigh distillation law for Cr-isotope fractionation, and using a range of fractionation factors for

bio-reduction and abiotic reduction by Fe(II) (e.g. Sikora et al., 2008; Døssing et al., 2011; Janssen et al., 2020; Li et al., 2022), the Cr(VI) reduction in the most fractionated waters results ranging between about 47% and 72% (Fig. 10).

Leaching experiments indicate that the Cr-rich coatings represent a secondary chromate source at Green Park. Even if the detailed mechanism responsible for the deposition of such coatings remains undefined, they likely formed by evaporative precipitation after flooding events. The $\delta^{53}Cr$ value of $+2.315 \pm 0.062$ ‰ measured in the Cr(VI) leachate indicates that hexavalent chromium in polluted water during evaporation underwent reduction to Cr(III). Upon evaporation, water became supersaturated allowing the formation of the observed surface precipitates which incorporated and/or adsorbed both Cr(III) and Cr(VI). Indeed, amorphous silica precipitates act as sorbent for Cr(III). The sorption process may result in surface nucleation of a chromium hydroxide phase with γ-CrOOH structure (Fendorf et al., 1994), a phase with the octahedral coordination of Cr(III), and/or precipitation of an amorphous Cr-silicates (Elliott et al., 2014). This is in agreement with both the Cr–Si relationship highlighted by EDS analysis and with XANES spectra where the main signal is compatible with octahedrally coordinated Cr(III). Hexavalent chromium might be incorporated as chromate group in calcite (Hua et al., 2007; Tang et al., 2007) and/or isomorphous substitution for the SO_4 group in sulfate, such as gypsum (Morales et al., 2016) detected in coatings.

Hexavalent Cr pollution at Green Park poses direct threats to human health. Indeed, the comparison of risk based SSL with the concentration measured on site, indicates that the main health threat is associated with the presence of Cr(VI) and the most critical exposure pathways are both ingestion and dermal contact. Inhalation doesn't give rise to potential adverse health effects. However, it must be stressed that for inhalation the risk assessment was exclusively related to the emission flux of particulate from soil sources and does not include other types of emissions such as road transport, including non-exhaust particulate. Calculations indicate that total chromium concentration (considered as Cr(III)) would not produce any significant health risk even at concentrations much higher than the threshold imposed by Italian regulations for residential soil.

It is worth noting that the calculated SSL value is based on a precautionary target cancer risk of 10^{-6}. Indeed, risk assessments carried out following international guidelines are often based on multiple conservative assumptions and default exposure parameters which represent reasonable maximum exposure conditions for long-term/chronic exposure. This approach may lead to an extremely conservative Cr(VI) soil screening level (Proctor et al., 1997) yielding over-estimated remedial goals. Even if the SSL concentration value for Cr(VI) obtained in this study may be intended as cautionary, it is interesting to note that it is lower than the Cr(VI) concentration threshold imposed by Italian regulations for soil quality. This observation raises the basic question about the actual validity of the regulatory threshold value for Cr(VI) in soil for an adequate protection of public health, and highlights the need for site-specific health risk assessments.

7. Conclusions

This study has shown that the uncontrolled reuse of pyrolyzed tannery waste material generated from leather processing (KEU) may pose environmental and human health problems, due to the release of harmful pollutants to soil and water, in particular highly toxic Cr(VI). KEU, mixed to form an aggregate material used for road construction in the residential area Green Park in Tuscany (Italy), became a source of Cr. The chromium released from KEU has an anthropogenic origin, and as such, it does not contribute to the natural background. Instead, it adds to the anthropogenic environmental burden. Trivalent Cr in KEU partly oxidized to the hexavalent form Cr(VI) which was mobilized and dispersed in soil and roadways during rainfalls, representing secondary sources of contamination. The Cr-isotope and concentration data indicate that hexavalent chromium underwent reduction and dilution processes to different extents. Intense rainfalls and long drainage duration could extend the contamination to the deeper aquifers and to the floodplain outside the Green Park area, requiring mitigation measures to avoid further and more extensive environmental damages in the future. Indeed, the alternating wetting and drying conditions and the flooding events during rainstorms influence the fate of Cr contamination and the dynamics of migration. Risk assessment indicates that the Cr(VI) soil contamination might have deleterious health impacts on Green Park residents. It is worth to note that the obtained screening level values for Cr(VI) are significantly lower than the threshold imposed by Italian regulations for residential settings, raising concerns about the effectiveness of the concentration threshold imposed by environmental regulations in protecting human health.

CRediT authorship contribution statement

Lisa Ghezzi: Writing – review & editing, Writing – original draft, Validation, Investigation, Formal analysis, Data curation, Conceptualization. **Simone Arrighi:** Writing – original draft, Software, Data curation. **Enrico Mugnaioli:** Writing – original draft, Formal analysis, Data curation. **Natale Perchiazzi:** Writing – original draft, Software, Data curation. **Erika Zamponi:** Formal analysis. **Simone Pollastri:** Methodology, Formal analysis. **Fabrizio Franceschini:** Data curation. **Riccardo Petrini:** Writing – original draft, Visualization, Validation, Supervision, Resources, Project administration, Conceptualization.

Declaration of competing interest

The authors declare that they have no known competing financial interests or personal relationships that could have appeared to influence the work reported in this paper.

Data availability

Data will be made available on request.

Acknowledgements

Authors thank the Center for Instrument Sharing of the University of Pisa (CISUP) for giving access to HR-TEM facilities.

References

Amorosi, A., Sammartino, I., Sarti, G., 2013. Background levels of potentially toxic metals from soils of the Pisa coastal plain (Tuscany, Italy) as identified from sedimentological criteria. Environ. Earth Sci. 69, 1661–1671.
Apte, A.D., Verma, S., Tare, V., Bose, P., 2005. Oxidation of Cr(III) in tannery sludge to Cr (VI): field observations and theoretical assessment. J. Hazard Mater. 121, 215–222.
Arcibar-Orozoco, J.A., Barajas-Elías, B.S., Baltazar-Campos, H., Rangel-Mendez, R., 2022. Preparation of carbon materials from chromium-tanned leather shavings for the removal of dyes from aqueous solution. Appl. Water Sci. 12, 213.
ASTM, 2000. Report E 2081-00; Standard Guide for Risk-Based Corrective Action. American Society for Testing Materials: West Conshohocken, PA, USA.
Bongers, A., Casas, P., 2022. The circular economy and the optimal recycling rate: a macroeconomic approach. Ecol. Econ. 199, 107504.
China, C.R., Maguta, M.M., Nyandoro, S.S., Hilonga, A., Kanth, S.V., Njau, K.N., 2020. Alternative tanning technologies and their suitability in curbing environmental pollution from the leather industry: a comprehensive review. Chemosphere 254, 126804.
Chojnacka, K., Skrzypczak, D., Mikula, K., Witek-Krowiak, A., Izydorczyk, G., Kuligowski, K., Bandrow, P., Kułazynski, M., 2021. Progress in sustainable technologies of leather wastes valorization as solutions for the circular economy. J. Clean. Prod. 313, 127902.
Corti, G., Ugolini, F.C., Agnelli, A., 1998. Classing the soil skeleton (greater than two millimeters): proposed approach and procedure. SoilScience Society of America Journal 62, 1620–1629.
Cowherd, C., Muleski, G.E., Englehart, P.J., Gillett, D.A., 1985. Rapid assessment of exposure to particulate emissions from surface contamination sites, midwest research institute. In: PB85-192219.

Das, S., Lee, S.-H., Kumar, P., Kim, K.-H., Lee, S.S., Bhattacharya, S.S., 2019. Solid waste management: scope and the challenge of sustainability. J. Clean. Prod. 228, 658–679.
Dinelli, E., Cortecci, G., Lucchini, F., Zantedeschi, E., 2005. Sources of major and trace elements in the stream sediments of the Arno river catchment (northern Tuscany, Italy). Geochem. J. 39, 531–545.
Dixit, S., Yadav, A., Dwivedi, P.D., Das, M., 2015. Toxic hazards of leather industry and technologies to combat threat: a review. J. Clean. Prod. 87, 39–49.
Døssing, L.N., Dideriksen, K., Stipp, S.L.S., Frei, R., 2011. Reduction of hexavalent chromium by ferrous iron: a process of chromium isotope fractionation and its relevance to natural environments. Chem. Geol. 285, 157–166.
Elci, L., Divrikli, U., Akdogan, A., Hol, A., Cetin, A., Soylak, M., 2010. Selective extraction of Cr(VI) using a leaching procedure with sodium carbonate from some plant leaves, soil and sediment samples. J. Hazard Mater. 173, 778–782.
Elliott, P., Giester, G., Rowe, R., Pring, A., 2014. Putnisite, $SrCa_4Cr_8^{3+}(CO_3)\,8SO_4(OH)\,16\cdot 25H_2O$, a new mineral from Western Australia: description and crystal structure. Mineral. Mag. 78, 131–144.
Ellis, A.S., Johnson, T.M., Bullen, T.D., 2002. Chromium isotopes and the fate of hexavalent chromium in the environment. Science 295, 2060–2062.
Famielec, S., 2020. Chromium concentrate recovery from solid tannery waste in a thermal process. Materials 13, 1533i.
Fendorf, S.E., Lamble, G.M., Stapleton, M.G., Kelley, M.J., Sparks, D.L., 1994. Mechanisms of chromium(III) sorption on silica. 1. Cr(III) surface structure derived by extended X-ray absorption fine structure spectroscopy. Environ. Sci. Technol. 28, 284–289.
Fendorf, S.E., Eick, M.J., Grossi, P., Sparks, D.L., 1997. Arsenate and chromate retention mechanisms on goethite. 1, Surface structure. Environ. Sci. Technol. 31, 315–320.
Gates-Rector, S., Blanton, T, 2019. The powder diffraction file: a quality materials characterization database. Powder Diffr 34, 352–360.
Ghezzi, L., Mugnaioli, E., Perchiazzi, N., Duce, C., Pelosi, C., Zamponi, E., Pollastri, S., Campanella, B., Onor, M., Abdellatief, M., Franceschini, F., Petrini, R., 2023. Hexavalent chromium release over time from a pyrolyzed Cr-braring tannery sludge. Sci. Rep. 13, 16283.
Guan, Y., Liu, C., Peng, Q., Zaman, F., Zhang, H., Jin, Z., Wang, A., Wang, W., Huang, Y., 2019. Pyrolysis kinetics behavior of solid leather wastes. Waste Manag. 100, 122–127.
Hu, Y., Liu, T., Chen, N., Feng, C., 2021. Iron oxide minerals promote simultaneous bio-reduction of Cr(VI) and nitrate: implications for understanding natural attenuation. Sci. Total Environ. 786, 147396.
Hua, B., Deng, B., Thornton, E.C., Yang, J., Amonette, J.E., 2007. Incorporation of chromate into calcium carbonate structure during coprecipitation. Water Air Soil Pollut. 179, 381–390.
ISPRA, 2008. Methodological criteria for absolute risk analysis application at contaminated sites. www.isprambiente.gov.it (July 2023).
Janssen, D.J., Rickli, J., Quay, P.D., White, A.E., Nasemann, P., Jaccard, S.L., 2020. Biological control of chromium redox and stable isotope composition in the surface ocean. Global Biogeochem. Cycles 34, 1–18.
Jardine, P., Stewart, M., Barnett, M.O., Basta, N.T., Brooks, S.C., Fendorf, S., et al., 2013. Influence of soil geochemical and physical properties on chromium (VI) sorption and bioaccessibility. Environ. Sci. Technol. 47, 11241–11248.
Karydas, A.G., et al., 2018. An IAEA multi-technique X-ray spectrometry endstation at Elettra Sincrotrone Trieste: benchmarking results and interdisciplinary applications. J. Synchrotron Radiat. 25, 189–203.
Khan, A.A., Muthukrishnan, M., Guha, B.K., 2010. Sorption and transport modeling of hexavalent chromium on soil media. J. Hazard Mater. 174, 444–454.
Kim, C., Zhou, Q., Deng, B., Thornton, E.C., Xu, H., 2001. Chromium(VI) reduction by hydrogen sulfide in aqueous media: stoichiometry and kinetics. Environ. Sci. Technol. 35, 2219–2225.
Kitchen, J.W., Johnson, T.M., Bullen, T.D., Zhu, J., Raddaz, A., 2012. Chromium isotope fractionation factors for reduction of Cr(VI) by aqueous Fe(II) and organic molecules. Geochem. Cosmochim. Acta 89, 190–201.
Laurenti, R., Redwood, M., Puig, R., Frostell, B., 2016. Measuring the environmental footprint of leather processing technologies. J. Ind. Ecol. 21, 1180–1187.
Li, Y., Huang, Y., Li, Z., Tang, X., Liu, X., Hughes, S.S., 2022. Mechanisms of chromium isotope fractionation and the applications in the environment. Ecotoxicol. Environ. Saf. 242, 113948.
Liu, Q.liu, Liu, H., Chen, H., Wang, X., Hu, D., Cheng, X., Xu, H., 2020. Thermodynamic investigation with chemical kinetic analysis on the reoxidation phenomenon of the Cr (III) in air. RSC Adv. 10, 27775–27787.
Liu, X., Chen, X., Zhang, X., Guo, H., Zhang, C., Zang, X., Li, B., 2021. Quantifying the influence of soil factors on the migration of chromium(VI). Process Saf. Environ. Protect. 155, 32–40.
Mella, B., Glanert, A.C., Guterres, M., 2015. Removal of chromium from tanning wastewater and its reuse. Process Saf. Environ. Protect. 95, 195–201.
Morales, J., Astilleros, J.M., Matesanz, E., Fernández-Díaz, L., 2016. The growth of gypsum in the presence of hexavalent chromium: a multiscale study. Minerals 6, 22.
Panichev, N., Mandiwana, K., Foukaridis, G., 2003. Electrothermal atomic absorption spectrometry determination of Cr(VI) in soil after leaching of Cr(VI) species with carbon dioxide. Anal. Chim. Acta 491, 81–89.
Pettine, M., D'Ottone, L., Campanella, L., Millero, F.J., Passino, R., 1998. The reduction of Cr(VI) by iron (II) in aqueous solutions. Geochem. Cosmochim. Acta 62, 1509–1519.
Pontér, S., Pallavicini, N., Engström, E., Baxter, D.C., Roduskin, I., 2016. Chromium isotope ratio measurements in environmental matrices by MC-ICP-MS. J. Anal. At. Spectrom. 31, 1464–1471.
Proctor, D.M., Shay, E.C., Scott, P.K., 1997. Health-based soil action levels for trivalent and hexavalent chromium: a comparison with state and federal standards. J. Soil Sedim. Contam. 6, 595–648.
Ravel, B., Newville, M., Athena, A.H., 2005. Data analysis for X-ray absorption spectroscopy using IFEFFIT. J. Synchrotron Radiat. 12, 537–541.
Rosu, L., Varganici, C.D., Crudu, A.M., Rosu, D., Bele, A., 2018. Ecofriendly wet–white leather *vs* conventional tanned wet–blue leather. A photochemical approach. J. Clean. Prod. 177, 708–720.
Shervais, J.W., 1982. Ti-V plots and the petrogenesis of modern and ophiolitic lavas. Earth Planet Sci. Lett. 59, 101–118.
Sikora, E.R., Johnson, T.M., Bullen, T.D., 2008. Microbial mass-dependent fractionation of chromium isotopes. Geochem. Cosmochim. Acta 72, 3631–3641.
Sivaram, N.M., Barik, D., 2019. Toxic waste from leather industries. In: Barik, D. (Ed.), Energy from Toxic Organic Waste for Heath and Power Generation. Woodhead Publishing, pp. 55–67.
Tang, Y., Elzinga, E.J., Lee, Y.L., Reeder, R.J., 2007. Coprecipitation of chromate with calcite: batch experiments and X-ray absorption spectroscopy. Geochem. Cosmochim. Acta 71, 1480–1493.
Tasca, A.L., Puccini, M., 2019. Leather tanning: life cycle assessment of retanning, fatliquoring and dyeing. J. Clean. Prod. 226, 720–729.
US EPA, 1996. Soil screening guidance: technical background document. Office of Emergency and Remedial Response. US Environmental Protection Agency, Washington, DC, USA, EPA/540/R-95/128.
US EPA, 2002. Supplemental Guidance for Developing Soil Screening Levels for Superfund Sites; OSWER 9355, vols. 4–24. US Environmental Protection Agency; Office of Emergency and Remedial Response, Washington, DC, USA.
US EPA, 2004. Risk assessment guidance for superfund. Volume I. Human Health Evaluation Manual, Part E. US Environmental Protection Agency; Office of Superfund Remediation and Technology Innovation, Washington, DC, USA, EPA/540/R-99/005.
US EPA, 2009. Risk Assessment Guidance for Superfund—Volume I: Human Health Evaluation Manual (Part F, Supplemental Guidance for Inhalation Risk Assessment); U.S.EPA-540-R-070-002; Office of Superfund Remediation and Technology Innovation. US Environmental Protection Agency, Washington, DC, USA.
US EPA, 2014. Human Health Evaluation Manual, Supplemental Guidance: Update of Standard Default Exposure Factors; OSWER Directive 9200.1-120; Office of Solid Waste and Emergency Response. US Environmental Protection Agency, Washington, DC, USA.
US EPA, 2023a. Regional screening levels (RSLs) - generic tables. US environmental protection agency. In: Washington, DC, USA. https://www.epa.gov/risk/regional-screening-levels-rsls-generic-tables. December 2023.
US EPA, 2023b. Regional Screening Level (RSLs)—Equations. US Environmental Protection Agency, Washington, DC, USA. https://www.epa.gov/risk/regional-screening-levels-rsls-equations#res (July 2023).
US TCEQ, 2023. TRRP PCL tables. Texas Commission of Environmental Quality. https://www.tceq.texas.gov/downloads/remediation/trrp/march-2023-pcl-tables.pdf. December 2023.
US UT, 2023. RAIS: risk assessment information system. Chemical Risk Calculator User's Guide. https://rais.ornl.gov/tools/rais_chemical_risk_guide.html. December 2023.
Verma, S.K., Sharma, P.C., 2022. Current trends in solid tannery waste management. In: Critical Reviews in Biotechnology. Taylor and Francis Ltd.
Wielinga, B., Mizuba, M.M., Hansel, C.M., Fendorf, S., 2001. Iron promoted reduction of chromate by dissimilatory Iron-reducing bacteria. Environ. Sci. Technol. 35, 522–527.
Whitaker, A.H., Peña, J., Amor, M., Duckworth, O.W., 2018. Cr(VI) uptake and reduction by biogenic iron (oxyhydr)oxides. In: Environ. Sci. Processes Impacts 20, pp. 1056–1068.
Wittbrodt, T., Palmer, C.D., 1995. Reduction of Cr(VI) in the presence of excess soil fulvic acid. Environ. Sci. Technol. 29, 1–25.